Contents lists available at ScienceDirect

South African Journal of Chemical Engineering

journal homepage: http://www.journals.elsevier.com/south-african-journal-of-chemical-engineering

Analysis of catalyst photo-oxidation selectivity in the degradation of polyorganochlorinated pollutants in batch systems using UV and UV/TiO_2

*Zack Khuzwayo**, *Evans M.N. Chirwa*

Department of Chemical Engineering, Water Utilisation Division, University of Pretoria, Pretoria, 0002 South Africa

ARTICLE INFO

Article history:
Received 21 June 2016
Received in revised form
27 September 2016
Accepted 23 December 2016

Keywords:
Photocatalysis
Photolysis
Organochlorides
Chlorobiphenyls
Batch-reactor

ABSTRACT

Worldwide concerns of organic pollutant free water supply have attracted significant attention to the technological advances in water and wastewater treatment. Photocatalysis is one of the technologies that have been proven to be effective at degrading organic micro-pollutant to noble constituents. This study investigated the selective influence of structural conformations of multi-chlorohalogenated substituted organochloride compounds by TiO_2 as a semiconductor photocatalyst in the heterogeneous photocatalytic and photolytic treatments of organics in aqueous batch systems. The chemical compounds under scrutiny were DDT (dichlorodiphenyltrichloroethane), chlordane and 2.3.4-TCB (2.3.4-trichlorobiphenyl). Photo-induced oxidation profiles were determined to adhere to structural configuration preferential selectivity in favour of smaller sized molecular compounds, where chlordane achieved the least efficiency in removal. The photocatalytic degradation process indicated partial selectivity against chlordane in favour of DDT and TCB, where maximum efficiencies were recorded for the smaller molecular structure compounds, while chlordane recorded significantly lower efficiency of reduction. The photocatalytic performance relationship was that of impeded photon delivery with increased catalyst mass loading. The Langmuir–Hinshelwood expression was used to model the photocatalytic degradation process, where the adsorption parameters were calculated from photocatalyst isothermal adsorption studies. The reaction kinetic parameters were simulated and estimated using an aquatic systems modelling software.

1. Introduction

Many agricultural pesticides and chlorobiphenyls are found in the environment. The majority of pesticides gained popularity after the Second World War (Atoko et al., 2015; Chelme-Ayala et al., 2011; Kaushik and Kaushik, 2007), while chlorobiphenyls are a group of pollutant chemicals that were utilised in the manufacturing of electrical equipment and hydraulic systems (Hughes et al., 2015; Ishikawa et al., 2007), before stringent regulation and bans were imposed to both groups because of their acute toxicity, suspected endocrine, immuno- and neuro-toxicity, and bioaccumulation capabilities (Manickum and John, 2014; Marx-Stoelting et al., 2014; Selli et al., 2008). Many of these banned substances are still present in the environment and those under strict regulation are typically detected in higher concentrations than stipulated. South Africa still experiences a high number of persistent organic pollutants in the environment, though most of these

* Corresponding author.
E-mail address: zack.khuzwayo@up.ac.za (Z. Khuzwayo).
http://dx.doi.org/10.1016/j.sajce.2016.12.002

substances have been banned for many years (Ryan et al., 2012). Conventional and traditional water and wastewater treatment facilities are not adequately effective at treating most complex structure organic chemical groups. The representative group of compounds in this study are 1.1.1-trichloro-2.2-bis(4-chlorophenyl)ethane (DDT), chlordane and 2.3.4-trichlorobiphenyl.

One of the more effective technologies in dealing with emerging pollutants are advanced oxidation processes (AOPs), as they are generally non-selective and are capable of completely mineralising most organic chemical species (Ângelo et al., 2013; Demeestere et al., 2007; Carp et al., 2004). Advanced oxidation degradation of organic pollutants is achieved by generation of free hydroxyl (OH°) radicals using various technologies such as and a combination including ozonation, ultra-violet (UV) light, semiconductor photocatalysts, hydrogen peroxide, ultra-sound, and Fenton reagent (Levya-Diaz et al., 2015; Suzuki et al., 2015). Photocatalysis is one of the techniques that have found diverse applications in the treatment of persistent organic micro-pollutants. The nucleus of the photocatalytic concepts is embedded on the generation of energy bandgaps upon photon excitation of semiconductor materials. When light photons of a sufficient quantum and corresponding wavelength comes into contact with electrons on material surfaces such as semiconductors, the energy carried by the photons is absorbed, which results in the electrons moving to a higher energy state (conduction band). The absorbed energy can be relinquished by the electrons and dissipated in the form of photon energy, this result in electron descent to lower orbitals where they settle at characteristic ground energy states (valence band). This is referred to as electron hole pairs recombination, the recombination of the generated charges competes and minimises the trapping of free ionic chargers. The facilitation of effective photocatalytic degradation requires that the recombination of the electron and positive hole be prevented through reaction inhibitors in the form of electron donors and electron acceptors. Oxygen is the primary electron acceptor that is typically utilised for the purposes of trapping electrons in photocatalysis. The oxygen molecule reacts with free electrons and is converted to superoxide upon acceptance and trapping of the electrons. The remaining surface bound positive hole though radical formations facilitate oxidation pathways.

A limited number of studies have been conducted on the simultaneous oxidation of different classes of organochloride compounds and their relative performance with regards to photocatalyst adsorption selectivity. In this study, three structurally dissimilar organochloride compounds will be analysed for photolytic and photocatalyst structural selectivity, Fig. 1 shows the molecular structures of the 3 selected compounds, the red and blue moieties are a depiction of the chemical symmetry of the compounds that indicates the same substitution in either of the ring structures. Chemical molecular structures have been reported to have an influence on the rate of photocatalytic oxidation (Ji et al., 2013). Palmisano et al. (2007) studied how different benzene derivatives substituent groups affect the photocatalytic selectivity to hydroxylated compounds, and found that molecular compounds with strong electron withdrawing groups are adsorbed better. Halogen dechlorination of the base-structures of the DDT, chlordane and 2.3.4-trichlorobiphenyl will be analysed for titanium dioxide (TiO_2) catalyst induced photo-reactivity and their rate of reactions. The effectiveness of photocatalytic advanced oxidation of related chemical groups is well documented in scientific literature, but limited resources have been dedicated to the determination of unrelated group of chemicals. The reason is that unrelated compound groups provide a bigger challenge in that molecular transformations are not easily tracked and kinetic feedback is subjected to a high degree of speculation.

This is because molecular forces of liquid–solid interfaces in heterogeneous reactions are subjected to photocatalyst chemical adsorption thermodynamic limitations (Chakraborty and Sun, 2014; Song et al., 2013), coupled with various Langmuir adsorption isotherms assumptions. One important Langmuir assumption is that, a fixed number of vacant or adsorption sites are available on the solid catalyst surfaces, meaning that as more sites on substrate are filled it becomes increasingly difficult for a bombarding solute molecule to find vacant sites (Giles et al., 1960). There is also the principle of catalyst selectivity that is dependent on the structure of specific chemical groups and their variability (Tatsumi et al., 1993). Experimental data will be used to determine the oxidation behaviour of the three compounds to and correlations between compound structural details and the degradation efficiency with respect to the semiconductor

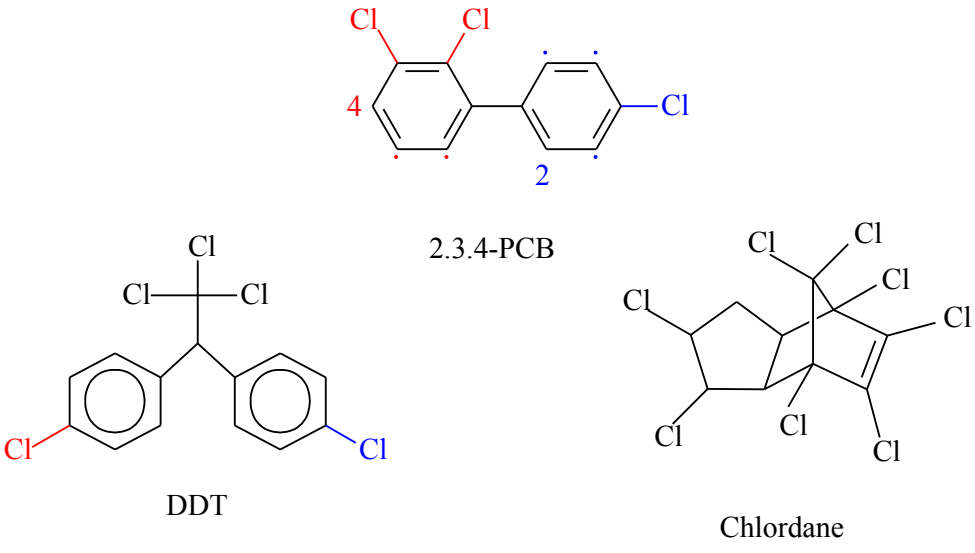

Fig. 1 – Molecular structures of DDT, 2.3.4-PCB and chlordane.

catalyst adsorption capacity. The orders of the rate of photolytic reactions will be investigated, as well as the Langmuir–Hinshelwood kinetics used to estimate kinetic parameters.

Photocatalysis and photolysis are advanced oxidation process technologies that have garnered significant interest in the last couple of decades. Many studies have been conducted on the subject and the majority of findings demonstrate superiority of photocatalysis over photolysis in the efficiency of chemical treatment. It is however very difficult to measure performance differences of the two applications in isolation when dealing with lower mass organic compounds, and this has been evident in studies by Chun et al. (2000) and Mohseni (2005). The photo-induced semiconductor catalyst oxidation process cannot be evaluated in separation from the simple parts of its principle precursor, which are photolysis and the formation of hydroxyl radicals in the absence of the catalyst. The effects of all the degradation processes in isolation, though near impossible to quantify separately are additive in the overall resultant photocatalytic process. The degradation pathways and reaction schemes preferred may encompass the complete range of possible oxidation routes for both oxidation processes. It can however be theoretically possible to ascribe difference by evaluating the mechanistic oxidation pathways followed, the major assumption would be that each process strictly follows independent reaction schemes, and there has not been evidence to support this fully. There however has been information to suggest that compound specific semiconductor photocatalyst selectivity play a role in the efficiency of chemical treatment.

2. Methods

2.1. Chemicals

DDT (99.9%), chlordane (99.7%), and 2.3.4-PCB (TCB) (99%) were obtained from Sigma–Aldrich Logistik GmbH (Schnelldorf, Germany). Aeroxide P25 anatase titanium dioxide was purchased from Evonik Degussa GmbH (Japan). Ultra-pure (UP) water was dispensed by the Millipore Direct Q3 with pump instrument. High Purity Pesticide Reference standard were purchased (N9331029) from PerkinElmer (South Africa division), GC grade MeOH obtained from Merk (South Africa).

2.2. Instrumentation

Polychlorinated phenolics and derivative products were analysed using a gas chromatography (GC) system comprising of a clarus 600 GC, clarus 600T mass spectrometer (MS), attached to a turbomatrix 40 trap headspace sampler (PerkinElmer, South Africa division). The chemical separation component was the Elite 5MS GC system capillary column (30 m, 250 μm) from PerkinElmer. Helium (He) carrier gas of 99.999% purity and applied at a flow rate of 1 ml min^{-1}. MS interface comprised of an Electron Ioniser (EI) and a high performance mass analyser.

2.3. Data processing, kinetic and modelling

Sigmaplot 11 scientific data analysis graphics computation software was used for data processing and statistical analysis. Aquasim 2.0 computer program for the identification and simulation of aquatic systems was used to simulate and model the photocatalytic oxidation profiles, and parameter estimations.

2.4. Equilibrium isotherms

Adsorption isotherms were determined by; accurately weighed titanium dioxide (0.005, 0.01, 0.02, 0.03 and 0.05 g l^{-1}) dispensed in aqueous polyorganochloride spiked (5, 10, 20, 30, 50 mg l^{-1}) solutions (0.5 l) continuously stirred at 300 rpm. The temperature was controlled at 19 °C. The resulting pH of the solutions was in within the range of 5.4–5.7. The solutions were agitated for over 20 h to reach equilibrium. After a minimum period of 20 h samples were removed and centrifuged (eppendorf AG minispin) for 30 min at 5000 rpm. Sample residual concentrations were analysed using the GCMS. Experiments were repeated and average values are reported. Langmuir isotherm models were used to calculate adsorption parameters.

2.5. Reactor configuration

The setup was installed in a temperature regulated walk-in reactor room that is wall-connected to a cold room of 4 °C set temperature. The wall connection has port-openings that allow transfer of cooled air for secondary cooling, driven by a pressure–vacuum system. Fig. 2 shows the setup layout; a cooling jacketed glass vessel was rested on a magnetic stirrer (Labex FMX electronics (STR-mH)). The jacket vessel was joint-linked to a MasterFlex console drive pump (Cole–Parmer instruments (Easy Load II)) and connected to an ice-water slurry feed for primary cooling. Suspended above the solution surface was a tube quart glass sleeve of 4 cm diameter. Encased in the quartz glass sleeves were long-arc 400 W (Philips HOK 4/120 SE) medium pressure lamps, details in Table 1. An oxygen inlet ((O_2) of 99% purity) delivery tube through a regulator was connected to a solution submerged longitudinal fizzle nozzle.

2.6. Experimental procedure

Source solutions were prepared in amber-glass vessels by spiking ultra-pure water with organochlorinated chemical reagents to approximate concentrations of 10 mg l^{-1} of each compound. The photocatalyst particle mass concentrations of 5, 10, 30, 50 and 200 mg l^{-1} were dispensed into solutions for the relevant experimental sets, this was followed by ultrasonication for a period of 15 min before transfer onto a magnetic stirrer that was set at 200 rpm, and the same was performed for the photolysis sets. Pure oxygen was delivered through nozzle outlets with a set flow-rate of 20 ml min^{-1}, the gas was turned on before solution delivery for optimum uninterrupted bubbling. After the zero-time sample, the UV source lamp was initiated. Sampling took place at predetermined intervals for total periods of 30 min. All sets were conducted in triplicates. Experiments start-up included pressurised air flow, continuous magnetic stirring, and continuous water flow cooling, and a dark period of 15 min. A Clarus Trap headspace was used for sample pre-concentration using high pressure extraction.

2.7. Instrumental analysis

5 ml samples were removed and pre-concentrated using a headspace trap. Headspace sample preparation: Temperature; needle 100 °C, transfer line 150 °C, oven 90 °C, trap low 80 °C, trap high 280 °C. Times; dry purges 5 min, trap hold 6 min, desorb 0.5 min, thermostat 40 min, GC cycle run 40 min, pressurization 1 min, decay 1 min. Pressures; column 25 psi, vial 20 psi, desorb 10 psi.

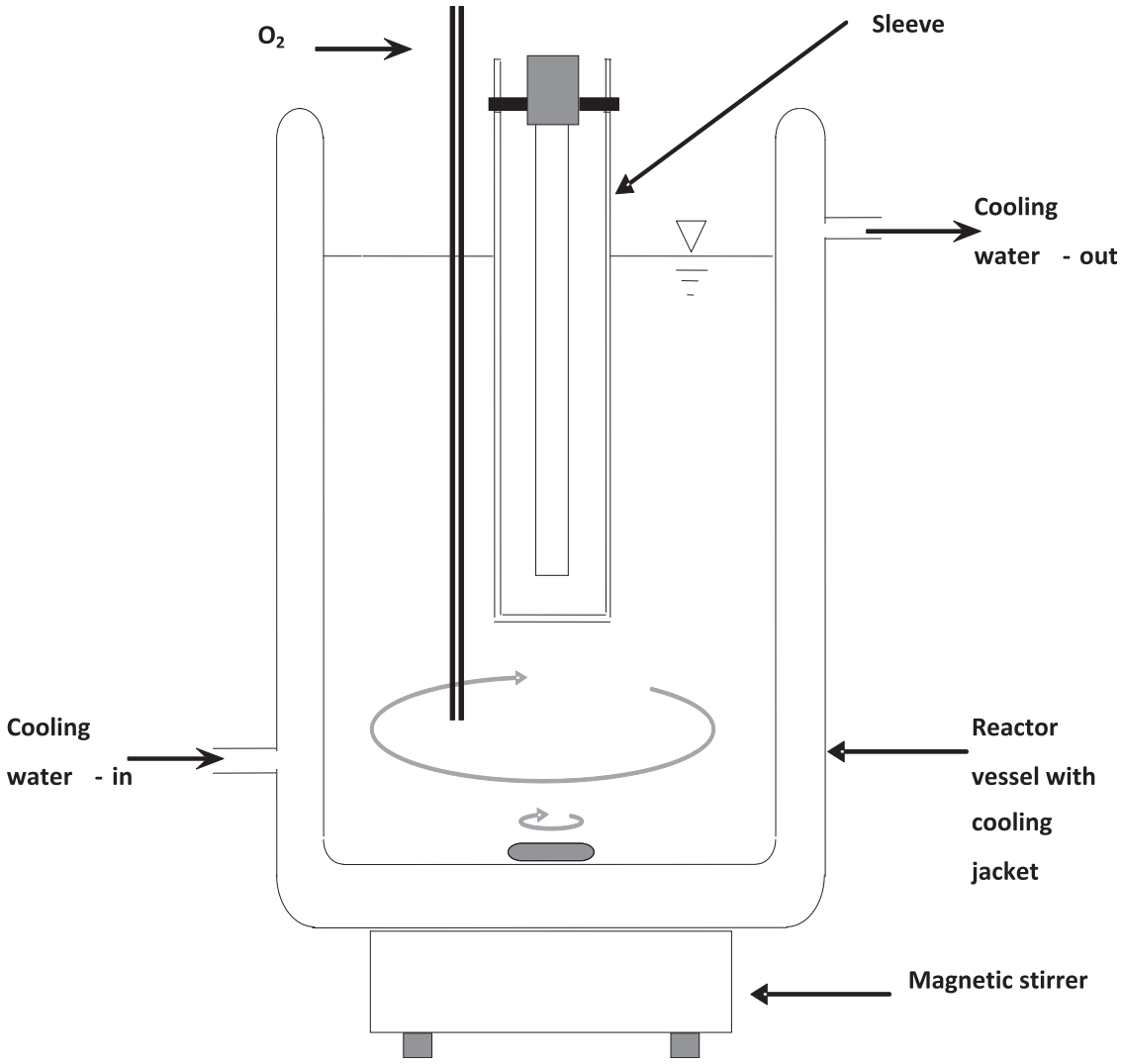

Fig. 2 – Schematic of the photo-oxidation reactor configuration.

Pre-concentrated samples were automatically transferred to the column. GC settings: Oven program; 50 °C held 2 min, ramped 10 °C min^{-1} until 300 °C, held 5 min. MS settings; mass range 30–450, source temperature 200 °C, multiplier 350 V.

3. Results

3.1. *Adsorption isotherms*

The Langmuir–Hinshelwood kinetic adsorption equilibrium isotherms of the three compounds of interest were calculated using the expression represented in Eq. (1a) where Q_e is the adsorbed chemical concentration per weight of adsorbent at equilibrium (mg g^{-1}), C_e is the final equilibrium solution concentration (mg l^{-1}), K_L is the free energy Langmuir adsorption constant (mg l^{-1}), and Q_m is the maximum adsorption capacity (mg g^{-1}).

Table 1 – Lamp properties used to configure the reactor system.

Lamp	Length (mm)	Width (mm)	Radiation Details (W)				Voltage (V)
			Wattage	UVA	UVB	UVC	
HOK4/120	100	16	400	31	32	52	120

$$Q_e = \frac{Q_m K_L C_e}{1 + K_l C_e} \quad (1a)$$

$$\frac{1}{Q_e} = \frac{1}{Q_m K_L C_e} + \frac{1}{Q_m} \quad (1b)$$

The plots of the inverse of the adsorbed chemical concentration per weight (Q_e) versus the inverse of the final equilibrium solution concentration (C_e) yields a linear expression. This equation is represented in Eq. (1b). The linear equation parameters are used to calculate the adsorption isotherm parameters, most importantly the Langmuir adsorption constant. The linear expression was used to determine the parameters in Table 2, the determinations of the model limit were performed by using a modelling software

Table 2 – Parameters of Langmuir isotherms for the adsorption of organochlorides onto TiO_2.

Isotherm	TCB	DDT	Chlordane
K_L (mg l^{-1})	0.371	0.756	0.266
Q_m (mg g^{-1})	72.364	119.78	211.86
R^2	0.9899	0.9914	0.9939
Stdev	0.061	0.084	0.0921

and represented in the form of standard error determinations. Table 2 presents the calculated parameters for the adsorption of the TCB, DDT and chlordane onto titanium dioxide surface sites. The plots of the inverse of the adsorbed chemical concentration per weight (Q_e) versus the inverse of the final equilibrium solution concentration (C_e) were used for studying the adsorption data. The Langmuir adsorption constants (K_L) for all compounds were calculated as recorded in Table 2.

3.2. *Photo-oxidation performance*

One of the objectives of this study was to evaluate the performance of photocatalysis as an improved technology to photolysis. The interest was to determine chemical specific behaviour in compound profiles that may be associated with semiconductor adsorption selectivity towards the three polychlorinated compounds of differing ring structures. Figs. 3–5 show the treatment profiles of TCB, DDT and chlordane respectively, at different photocatalyst concentration applications.

All graphics presented include the photolytic performance profiles. It has been found that photolysis is adequately efficient at facilitating complete disappearance of certain organic

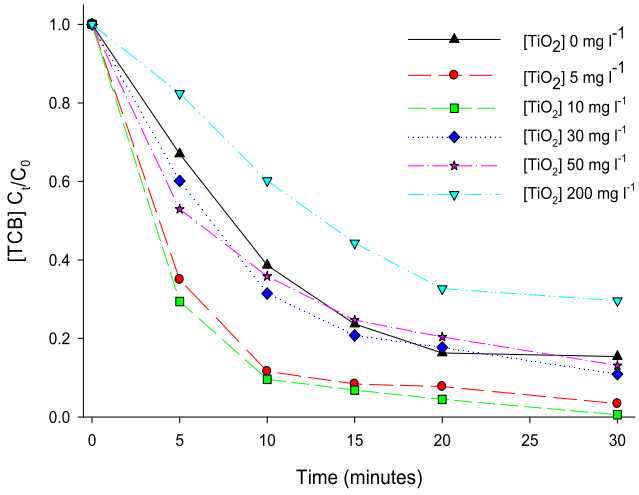

Fig. 3 – Photo-induced degradation of TCB in aqueous batch systems, 10 mg l^{-1}.

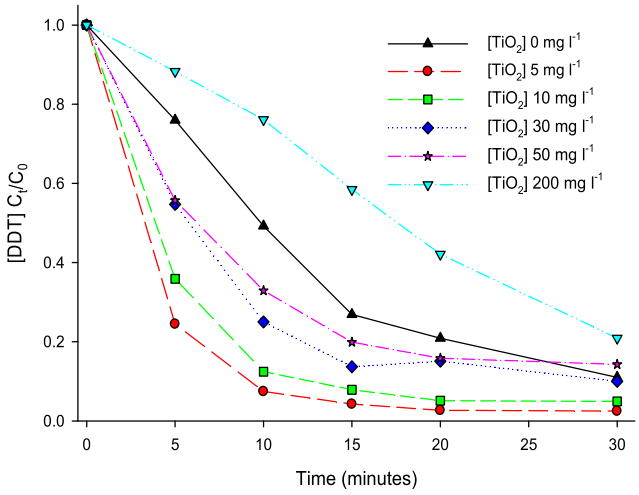

Fig. 4 – Photo-induced degradation of DDT in aqueous batch systems, 10 mg l^{-1}.

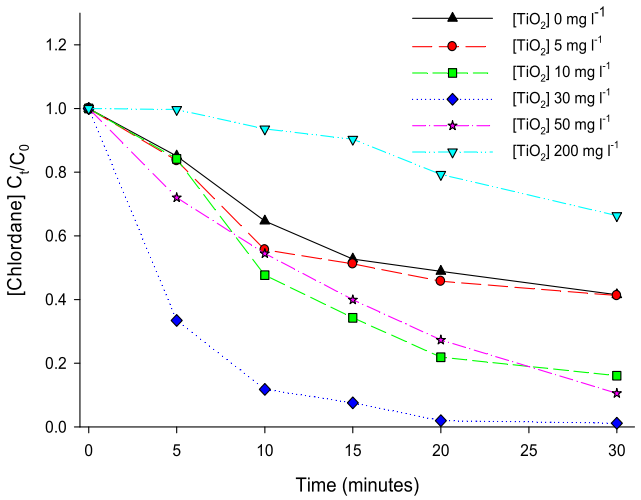

Fig. 5 – Photo-induced degradation of chlordane in aqueous batch systems, 10 mg l^{-1}.

compounds. This was reported by Liang et al. (2010) where it was also observed that though photolysis was efficient at degrading primary pollutants, it was very inefficient at complete mineralisation of intermediates species. An average of 61% of TCB was oxidised under photolysis conditions while over 90% was achieved by the 10 mg l^{-1} photocatalyst experimental sets, and over 88% in the 5 mg l^{-1} after 10 min of irradiation. Similarly to Fig. 3, an average of 51% of DDT was reduced in the first 10 min photolytically, while over 93% reduction was recorded by the 5 mg l^{-1} photocatalyst set in the same period. The 30 mg l^{-1} photocatalyst set was the most efficiently in Fig. 5, where the chlordane percent reduction registered over 88% and around 35% by photolysis in 10 min.

It is statistically justifiable to deduce that a significant reduction in the concentration of organics in solution is due to photolysis, though as indicated previously that this does not take place in isolation under semiconductor photocatalytic applications. It stands to reason that purely photolytic induced reaction pathways may form part of the overall oxidation reaction mechanisms. The photolytic process itself may be inclusive of solution-derived advanced oxidation process phenomena such as coupled UV/peroxide (H_2O_2) and UV/chloride, though the contributions of these processes are expected to be minimal. The relevance of the photolysis/chlorine coupling oxidation potential is based on the resultant free charged chloride ions in solution delivered by dehalogenation mechanistic reactions that are plausible in the photocatalyst concept. The peroxide molecule results from conduction band reductive reactions with the electron accepting oxygen molecule. The UV/peroxide coupling can produce strong hydroxyl radicals (HO°) that facilitate oxidation (Pan et al., 2015; Verbruggen, 2015).

Fig. 6 shows the reduction percentages of TCB, DDT and chlordane after a period of 15 min of irradiation in all the photocatalyst sets. The major elements to the photocatalytic principle in reactor design are mass transfer and photon delivery, which can greatly affect performance. Mass transportation in the photocatalytic context is the adsorption of organic molecules onto the photocatalyst surface, as a result of generated charged hydroxyl radical moieties. The theoretical basis is that the higher the number of available and activated semiconductor surface sites, the higher the efficiency of treatment. The oxide particles need activation to facilitate oxidation and reduction reactions, the activation process is

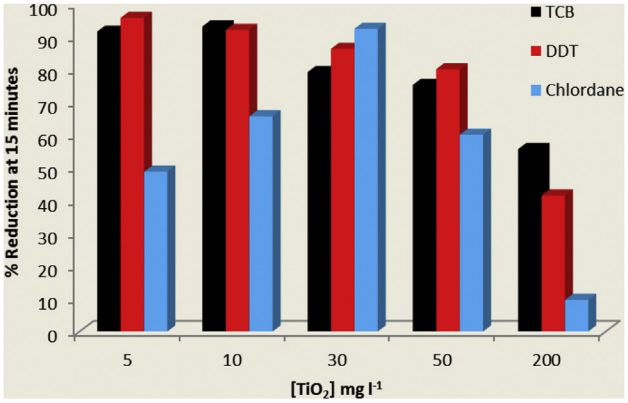

Fig. 6 – Photocatalytic percent reduction percentages at t = 15 min of irradiation.

initiated by the adsorption of photons generated from the irradiation source. In this study, by increasing the catalyst concentration, mass transfer is improved and concurrently the performance efficiency. However, mass transfer is improved at the expense of photon delivery. In suspended photocatalyst applications photon delivery is generally the limiting step, due to impaired and subsequently reduced photon radiation transmittance through translucent (murky) liquid mediums, affected by opaque solute particle properties and light scattering due to optical hindrance. All figures associated with the treatment of the three compounds show that at extreme higher photocatalyst concentrations such as the 200 mg l^{-1}, compounds reduction is significantly impaired. The main contributing factor to the impairment is the reduced solution transparency that is due to excessive amounts of solutes suspended in solution, and this applies equivalently for all compounds. This contribution is ubiquitous and can be removed from the analysis of photocalysts selectivity argument.

Fig. 6 shows that the highest achieved efficiencies for TCB and DDT were recorded around the 10 mg l^{-1} range, the next photocatalyst concentration point analysed was 30 mg l^{-1} which recorded approximately 13% decrease in efficiency. It can be collectively deduced that the optimum catalyst adsorption ranges for the TCB and DDT are below 20 mg l^{-1}, where closer inspection suggest TCB to be between 10 and 20 mg l^{-1} and DDT to be between 1 and 15 mg l^{-1} when statistical variance is applied. The paper by Liang et al. (2010) also suggested that the photocatalytic process has relatively poor selectivity towards specific compounds, and that the photolytic process has compound selective characteristics. The basis of selectivity or lack thereof can be a function of a combination of analyte compound factors, including compound molecular structural configuration, structural conformation, size, and bond structure properties. Given the closer similarity of the molecular structures of DDT and TCB, this could be a plausible explanation for the similarities in photocatalyst range efficiencies. DDT is made up of a 3-chloride junction joined to two aromatic rings that are substituted to a single chloride ion, while TCB is substituted with chloride ions with the most stable conformation being two chlorides on one aromatic ring and a single on the other. The accessibility from the structural conformation perspective to the titanium molecule may not be too different, nor the bond structure properties. Studies including that by Iraway et al. (2014) found that structural accessibility for the formation of the surface titania radical and molecule moiety bond play a pivotal role in determining the rate of reaction of the molecules, and that steric hindrances are factors that have major influences on rate of reactions.

Chlordane as is evident in Fig. 1 is a complex molecule, it is classified as a cyclodiene pesticide and is derived from hexachlorocyclopentadiene that undergoes chlorination. The relationship between photocatalyst loading and chlordane degradation is different to that registered for DDT and TCB, where lower concentrations of catalyst performed better and the efficiency was progressively compromised with increased loading beyond the estimation of 20 mg l^{-1}. It stands to reason that photon delivery is the sensitive factor in this regards, but chlordane reduction on the other hand improved with increases in catalyst loading, and achieved the highest efficiency at 30 mg l^{-1}. The explanation lies in the molecular structure of the compounds, DDT and TCB are relatively much less structurally hindered and better amicable at forming radical branched bonds in the transition steps of hydroxylation and subsequent release of the chloride ions.

Another mechanism that may be simultaneously undergone is the formation of hydroxyl-hydrogen bonds of less steric hindered carbons of the aromatic rings, this may result in numerous photocatalyst adsorbed junctions on the same molecule and oxidation taking place at all sites. Iraway et al. (2014) and Kang et al. (2002) reported such a hypothesis on the degradation of different functional groups. The chlordane molecular structure is conformationally less accessible and its photocatalyst adsorption is limited by this factor. The hypothesis is that at low photocatalyst loads, DDT, TCB and their derived intermediate compounds are favourably adsorbed and primarily occupy most of the limited number of available activated sites. Increases in the number of available sites improve the mass transfer potential but chlordane adsorption is still subjected to competition and is continuously outcompeted by the smaller molecules. It is only at sufficiently high catalyst loading that adequate number of sites are available for all smaller compounds to be adsorbed, and still remain enough activated sites to facilitate efficient adsorption and oxidation of chlordane. Photon delivery limitations are still experienced by the system, the expectations is that the most efficient chlordane rate of degradation will still be significantly less than those achieved by the structurally easier adsorbed compounds of DDT and TCB.

3.3. *Photolytic reaction kinetics*

Photolysis reaction schemes are generally assumed follow simple first-order kinetics, this is when direct photolysis is taken into account, without contributions of the radical pathways. In the first-order approximation the kinetic parameter represents the ratio between the total numbers of compound molecules degraded to the total number of photons absorbed by the compounds present in the solution. This simple reaction is represented in Eq. (2):

$$[OC] + h\nu \xrightarrow{\Phi I} [OC]_{oxid} \quad (2)$$

where Φ and I, are the quantum yield of the reaction and the radiation intensity, respectively, for the wavelength of the irradiation source that was used. A plot of Ln $[Conc]_0/[Conc]_t$ versus time of each compound results in a straight line with a slope that represents the degradation constant (k). Fig. 7 shows the confirmation of first-order rate of reaction kinetics. Table 3 shows the oxidation rate constants calculated from first-order

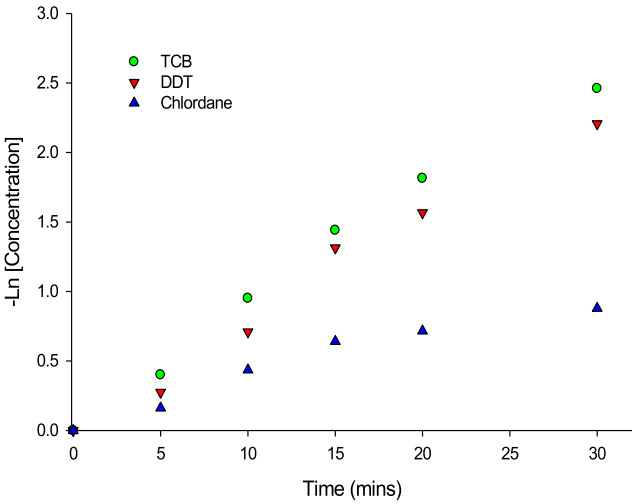

Fig. 7 – First-order photolytic oxidation determinations of TCB, DDT and chlordane.

Table 3 – First-order photolytic rate of degradation kinetic constants.

Analyte	Calculated *k*	Correlation coefficient	Simulated *k*
TCB	0.0840	0.9888	0.088152
DDT	0.0767	0.9854	0.074760
Chlordane	0.0303	0.9349	0.035965

k-mg l^{-1} min^{-1}.

determinations and estimated using Aquasim 2.0, the aquatic systems modelling software. The results show acceptable data correlation, and the calculated and simulated estimates of the degradation rate constants are relatively closely match.

3.4. *Photocatalytic reaction kinetics*

Modelling semiconductor photocatalytic reaction rates is based on a number of mathematical statements that can be expressed by sets of ordinary differentials equations, these are sourced and modified from de Lasa et al. (2005). These equations are established for the key chemical species and therefore species' balances in photocatalytic reactors can be typically described as in Eq. (3), where V is the total reactor volume.

$$V\frac{dC_o}{dt} = \left[\sum_k V_{o,k}R_k\right]W_{ir} \tag{3}$$

C_o is the concentration of a singular analyte compound, $V_{o,k}$ is a dimensionless stoichiometric coefficient for the compounds involved in reaction step, k and R_k being the rate of photo-conversion of step k based on the unit weight of irradiated catalyst, W_{ir}. Eq. (3) has assumption associated with it, which are that the mass concentration of the catalyst is known, complete mixing is achieved, and the reactor is operated in batch mode. Eq. (3) can be rearranged and simplified, such as in the case of degradation of a single compound. The rate of photooxidation can then be expressed in terms of measurable parameters and variables of that particular pollutant.

$$r_1 = \frac{V}{W_{ir}}\frac{dC_o}{dt} = \sum_k V_{o,k}R_k \tag{4}$$

The consideration of Eqs. (3) and (4) leads to the advancement of the photocatalytic conversion rate models into a format that is expressed in Eq. (5).

$$\frac{dC_o}{dt} = \frac{-k_o^m C_o}{1+\sum_{j-1}^{n} C_j K_j} \tag{5}$$

where k_o represents the kinetic constants for the o specie and K_j is the adsorption constant for the species j or any other species present. This reaction kinetic approach takes into account the reactor configuration and the behaviour of the irradiated semiconductor under the system specific conditions. The catalyst surface adsorption concept is viewed as purely dependant on the interaction between the photon and the catalyst mass. This theoretical approach is no different to accepted models that express the heterogeneous photocatalysis mechanism. The most complete of these models is the Langmuir–Hinshelwood expression.

The Langmuir–Hinshelwood (L–H) model is the most commonly used kinetic expression to explain the kinetics of the heterogeneous catalytic processes (Kumar et al., 2008). The expression has been successfully used for heterogeneous photocatalytic degradation to determine the relationship between the initial degradation rate and the initial concentration of the organic substrate (Saien and Khezrianjoo, 2008). The L–H expression assigned for heterogeneous photocatalytic behaviour takes the form of Eq. (6), where r is the rate of the reaction, k is the rate of surface reaction constant, K_L is the Langmuir–Hinshelwood semiconductor adsorption equilibrium constant calculated and represented in Table 2, and C is the concentration of the analytes of interest. Aquasim, aquatic modelling software was used to simulate and estimate the Langmuir–Hinshelwood differential expression parameters. The simulation process is conducted by numerically integrating a system of ordinary and partial differential equations in time and simultaneously solving the algebraic equation. The model was used to express the rate of the photocatalytic oxidation reactions and the influence of the adsorption capacity of the semiconductor. The surface adsorption model limits were carried over and set from the values determined from the TiO_2 catalyst isothermal equilibrium adsorption calculated error limits in the form of standard deviations. It is expected that the adsorption constant values calculated under isothermal equilibrium values (Table 2) may deviate from the calculated value within the limit set. It is only when the limits set do not conform to the proposed model that the integrity model is in question. The estimated adsorption constant values represent in Table 4 show that there is relatively good agreeability between the calculated values and the data informed estimated values.

$$r = \frac{kKC}{1+KC} \tag{6}$$

Table 4 shows the estimated L–H parameters for the degradation of TCB, DDT and chlordane. The degradation rate constants recorded improvements on the photolysis experimental sets, and are in agreement with the observation depicted in the graphical profiles. The 5 and 10 mg l^{-1} registered the highest efficiency in DDT and TCB oxidation that was followed by significant attenuation in the higher catalyst loaded sets. Expectedly, chlordane degradation registered the highest efficiency at the 30 mg l^{-1} catalyst concentration, there therefore was a progressive increase in efficiency that reached maximum at a given photocatalyst range before system

Table 4 – Estimated parameters of the photocatalytic degradation of organochloride compounds.

[TiO_2]	TCB		DDT		Chlordane	
	k	K_L	k	K_L	k	K_L
5	0.723420	0.332888	0.544943	0.686732	0.226136	0.200991
10	0.849955	0.324474	0.405826	0.683151	0.237470	0.341708
30	0.381055	0.316900	0.251481	0.696498	0.276474	0.166306
50	0.363142	0.314306	0.210824	0.703227	0.227527	0.343426
200	0.186488	0.323653	0.076356	0.837167	0.050321	0.268416

[TiO_2] mg l^{-1}; k mg l^{-1} min^{-1}; K_L mg l^{-1}.

Table 5 – Intermediate organic compounds detected using mass spectrum.

Compounds detected	
p,p-DDE	2.3-Dichlorobenzoic acid
DDD	Hydroxy-2.4-dichlorobenzoic acid
4-Chlorobenzoic acid	2.4-Dichlorobenzoic acid
2.2-bis(4-chlorophenol) methane	

impairments in the form of photon delivery compromised oxidation. It is also important to note that the estimated rate of reaction constant for the highest efficient chlordane experiment was significantly less than those of DDT and TCB at their highest efficiency. This is in line with the hypothesis of the titanium dioxide photocatalyst adsorption preference to compound structural properties. The photocatalyst compound adsorption constants were consistent and well within the error range limits for the smaller sized molecules, chlordane's adsorption constants though also within calculated limits varied somewhat in different catalyst loaded sets.

3.5. *Intermediate products*

Within each triplicate run of every experimental set pH changes were tracked and recorded. Average values of starting solutions after sonication registered pH values of 6.52 (±0.08). Results showed that there were gradually fractional increases in pH readings towards the pH 7 neutral zone. There was a relationship between efficiency of treatment and the resultant pH changes, where high oxidation performances recorded the bigger changes in pH jumps in comparison to initial readings. Since the oxidation process was not conducted towards complete mineralisation, but rather tracked the reduction of the primary compounds, it can be reasonably assumed that multitudes of intermediate compounds were present in solutions.

Analysis of experimental chromatogram peaks were conducted using the Perkin Elmer Turbomass software and the NIST Library software. Barring the spectrum hits on the primary analytes, Table 5 shows the compound detected with a certain degree of confidence amongst a lot of background noise. All compounds in Table 5 were present in trace amounts, it is only with the aid of the total ion chromatogram (TIC) analyser that each peak with the relevant ions could be identified. Table 5 shows the only compounds detected though it is assumed that many more are present below instrument detectable limits.

4. Conclusion

The photodegradations of DDT, TCB and chlordane were conducted in the presence of direct UV irradiation and in combination with titanium dioxide semiconductor catalyst. The primary study objective was to determine the oxidation mechanism selectivity between the three structurally dissimilar organochlorinated compounds by catalyst load manipulation and tracking of the oxidation process. Findings support the hypothesised oxidation mechanism differences that were validated by kinetic studies through calculations and estimated parameters. The chlordane degradation process performance differed significantly from that of DDT and TCB, both from the photolytic process and the photocatalytic process, where its oxidation efficiencies were significantly less than those of DDT. The photocatalytic efficiency of DDT and TCB was best managed at low relative catalyst mass concentrations while chlordane required much higher mass concentration of titanium dioxide photocatalyst. First-order oxidation principles were followed by the photolytic determination, while the Langmuir–Hinshelwood model adequately justified the photocatalytic behaviour in the heterogeneous photocatalysis sets.

Acknowledgements

Funding: This work was supported by the Water Research Commission (WRC) of South Africa through the WRC Project No. K5/1717 awarded to Prof Evans M.N. Chirwa of the University of Pretoria.

References

Atoko, O., Oppong-Otoo, J., Osei-Fosu, P., 2015. Carcinogenic and non-carcinogenic risk of organochlorine pesticide residues in processed cereal-based complementary foods for infants and young children in Ghana. Chemosphere 132, 193–199.

Ângelo, J., Andrade, L., Madeira, L., Mendes, A., 2013. An overview of photocatalysis phenomena applied to NOx abatement. J. Environ. Manag. 129, 522–539.

Carp, O., Huisman, C., Reller, A., 2004. Photoinduced reactivity of titanium dioxide. Prog. Solid State Chem. 32, 33–177.

Chakraborty, A., Sun, B., 2014. An adsorption isotherm equation for multi-types adsorption with thermodynamic correctness. Appl. Therm. Eng. 72, 190–199.

Chelme-Ayala, P., El-Din, M.G., Smith, D.W., Adams, C.D., 2011. Oxidation kinetics of two pesticides in natural waters by ozonation and ozone combined with hydrogen peroxide. Water Res. 45, 2517–2526.

Chun, H., Yizhong, W., Hongxiao, T., 2000. Destruction of phenol aqueous solution by photocatalysis or direct photolysis. Chemosphere 41, 1205–1209.

Demeestere, K., Dewulf, J., Van Langenhove, H., 2007. Heterogeneous photocatalysis as an advanced oxidation process for the abatement of chlorinated, monocyclic aromatic and sulfurous volatile organic compounds in air: state of the art. Crit. Rev. Environ. Sci. Technol. 37, 489–538.

Giles, C.H., Macewan, T.H., Nakhwa, S.N., Smith, D., 1960. Studies in adsorption. Part XI. A system of classification of solution adsorption isotherms, and its use in diagnosis of adsorption

mechanisms and in measurements of specific surface areas of solids. J. Chem. Soc. 10, 3973–3993.
Hughes, A.S., Vanbriesen, J.M., Small, M.J., 2015. Impacts of PCB analytical interpretation uncertainties on dechlorination assessment and remedial decisions. Chemosphere 133, 61–67.
Iraway, W., Soetaredio, F., Ayucitra, A., 2014. Understanding the relationship between organic structure and mineralization rate of TiO_2-mediated photocatalysis. Procedia Chem. 9, 131–138.
Ishikawa, Y., Noma, Y., Mori, Y., Sakai, S., 2007. Congener profiles of PCB and a proposed new set of indicator congeners. Chemosphere 67, 1838–1851.
Ji, Y., Zhou, L., Ferronato, C., Salvador, A., Yang, X., Chovelon, J., 2013. Degradation of sunscreen agent 2-phenylbenzimidazole-5-sulfonic acid by TiO_2 photocatalysis: kinetics, photoproducts and comparison to structurally related compounds. Appl. Catal. B Environ. 140–141, 457–467.
Kang, N., Lee, D., Yoon, J., 2002. Kinetic modeling of Fenton oxidation of phenol and monochlorophenols. Chemosphere 47, 915–924.
Kaushik, P., Kaushik, G., 2007. An assessment of structure and toxicity correlation in organochlorine pesticides. J. Hazard. Mater. 143, 102–111.
Kumar, K., Porkodi, K., Rocah, F., 2008. Langmuir–Hinshelwood kinetics – a theoretical study. Catal. Commun. 9, 82–84.
de Lasa, H., Serrano, B., Salaisis, M., 2005. Photocatalytic Reaction Engineering. Springer Science, New York.
Levya-Diaz, J.C., Lopez-Lopez, C., Martin-Pascual, J., Munio, M.M., Poyatos, J.M., 2015. Kinetic study of the combined processes of a membrane bioreactor and a hybrid moving bed biofilm reactor-membrane bioreactor with advanced oxidation processes as a post-treatment stage for wastewater treatment. Chem. Eng. Process. Process Intensif. 91, 57–66.
Liang, H., Li, X., Yang, Y., Sze, K., 2010. Comparison of the degradations of diphenamid by homogeneous photolysis and heterogeneous photocatalysis in aqueous solution. Chemosphere 80, 366–374.
Manickum, T., John, W., 2014. Occurrence, fate and environmental risk assessment of endocrine disrupting compounds at the wastewater treatment works in Pietermaritzburg (South Africa). Sci. Total Environ. 468–469, 584–597.
Marx-Stoelting, P., Niemann, L., Ritz, V., Ulbrich, B., Gall, A., Hirsch-Ernest, K.I., Pfeil, R., Solecki, R., 2014. Assessment of three approaches for regulatory decision making on pesticides with endocrine disrupting properties. Regul. Toxicol. Pharmacol. 70, 590–604.
Mohseni, M., 2005. Gas phase trichloroethylene (TCE) photooxidation and byproduct formation: photolysis vs. titania/silica based photocatalysis. Chemosphere 59, 335–342.
Palmisano, G., Addamo, M., Augugliaro, V., Caronna, T., Di Paola, A., Lopez, E.G., Loddo, V., Marci, G., Palmisano, L., Schiavello, M., 2007. Selectivity of hydroxyl radical in the partial oxidation of aromatic compounds in heterogeneous photocatalysis. Catal. Today 122, 118–127.
Pan, L.M., Zhang, X., Wang, L., Zou, J., 2015. Controlling surface and interface of TiO_2 toward highly efficient photocatalysis. Mater. Lett. 160, 576–580.
Ryan, P., Bouwman, H., Moloney, C., Yuyama, M., Yuyama, M., 2012. Long-term decreases in persistent organic pollutants in South African coastal waters detected from beached polyethylene pellets. Mar. Pollut. Bull. 64, 2756–2760.
Saien, J., Khezrianjoo, S., 2008. Degradation of the fungicide carbendazim in aqueous solutions with UV/TiO_2 process: optimization, kinetics and toxicity studies. J. Hazard. Mater. 157, 269–276.
Selli, E., Bianchi, C.L., Pirola, C., Cappelletti, G., Ragaini, V., 2008. Efficiency of 1,4-dichlorobenzene degradation in water under photolysis, photocatalysis on TiO_2 and sonolysis. J. Hazard. Mater. 153, 1136–1141.
Song, X., Zhang, Y., Yan, C., Jiang, W., Chang, C., 2013. The Langmuir monolayer adsorption model of organic matter into effective pores in activated carbon. J. Colloidal Interface Sci. 389, 213–219.
Suzuki, H., Araki, S., Yamamoto, H., 2015. Evaluation of advanced oxidation processes (AOP) using O_3, UV, and TiO_2 for the degradation of phenol in water. J. Water Process Eng. 7, 54–60.
Tatsumi, T., Yako, M., Nakamura, M., Yuhara, Y., Tominaga, H., 1993. Effect of alkene structure on selectivity in the oxidation of unsaturated alcohols with titanium silicalite-1 catalyst. J. Mol. Catal. 78, L41–L45.
Verbruggen, S., 2015. TiO_2 photocatalysis for the degradation of pollutants in gas phase: from morphological design to plasmonic enhancement. J. Photochem. Photobiol. C Photochem. Rev. 24, 64–82.